7

Removal of Phase Singular Points to Create Digital Elevation Map

The phase map obtained in observation of Mount Fuji presented in Chapter 5 shows the reflection phase modulo 2π. Therefore, the fringe curves are contours showing the geography in the observation area. Given one knows the fact, one can imagine the landscape of Mount Fuji to some extent. Computers can perform a similar processing to yield a height map, which we call a digital elevation map (or digital elevation model: DEM). The process to unwrap the phase image wrapped within $-\pi$ to π is the *phase unwrapping*. The phase unwrapping is, however, known as a difficult process for conventional computers because of the existence of phase singular points. In this chapter, first we explain the singular points, which is a serious noise induced in the interferometric observation. Then we present a method to remove the singular points effectively by using a complex-valued neural network, and generate a high-quality DEM with a smaller calculation cost.

7.1 Phase Unwrapping

The phase unwrapping is explained as follows. As we discussed in Chapter 5, the phase map obtained in airborne / satellite observation using interferometric radars possesses information equivalent to the height of land surface. However, the phase values are *wrapped* into $-\pi$ to π. By unwrapping them using computers, we can obtain so-called digital elevation map (DEM). This process is the phase unwrapping.

However, the phase unwrapping is known as a difficult task in conventional computing. Figure 7.1 illustrates, a little more microscopically, the amplitude and phase observed in a similar observation [202]. In the phase image, we can find some points where the phase values have rotational components. That is to say, when we examine the phase value around the point, it increases in 2π unawares, or decreases in -2π. We call the point the *singular point* (SP). The main origin is interference noise. We can also find in the amplitude

A. Hirose: Complex-Valued Neural Networks, SCI 400, pp. 123–131.
springerlink.com

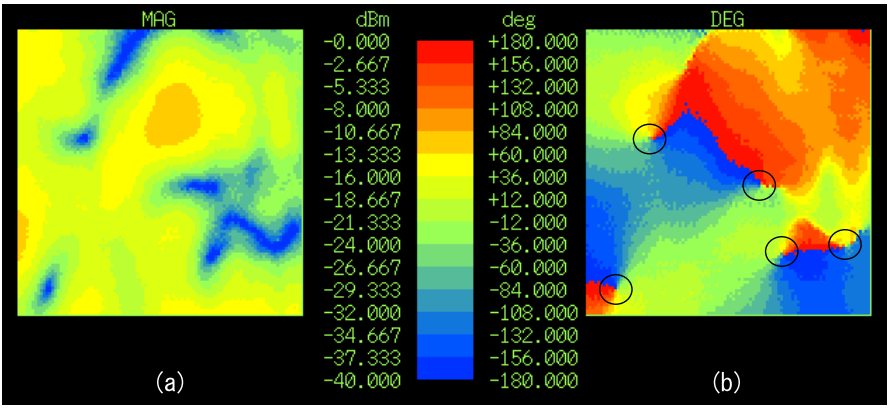

Fig. 7.1 Typical (a)amplitude and (b)phase images obtained by interferometric radars. In the phase image, we can find five phase singular points indicated by open circles. (Reprinted from Fig.3 in [202] with permission from Springer-Verlag.)

image that the points corresponding to the SPs have abrupt small values. The phenomenon is very natural since, in physical consideration, a point having indefinite phase value should not have any non-zero amplitude.

Because the phase value represents height of land surface, the phase field should intrinsically be conservative. Nonetheless, the field cannot be conservative actually. Then we cannot determine the height. For example, as we see later, the phase map shown in Fig.7.6(a) (Page 130) contains SPs of over 600.

However, we have a conventional method called the branch-cut method, so that we manage to determine, or more accurately, to estimate the height. In the branch-cut method, fundamentally we determine the height of a pixel by examining the phase shift between neighboring pixels, pixel by pixel, by incorporating 2π jump when we consider it appropriate. However, in this process, we place lines connecting SPs, and we determine the height without crossing the SP-connecting lines. In this way, regardless, we determine the elevation, though we have 2π cliffs on the SP-connecting lines because the line functions as a barrier of the spreading of the 2π inconsistency. Therefore, the total length of the lines should be as small as possible. When we connect all the SPs, the lines appear to be a branch in total. Hence the name branch-cut. The shorter the total length is, the better the DEM quality becomes. However, such a search problem with combinatorial explosion to find the shortest-line pairs is incompatible with ordinary computing. The computational cost grows seriously rapidly as the number of SPs increases.

t_{-12}	t_{-11}	t_{-10}	t_{-9}	t_{-8}
t_{-7}	t_{-6}	t_{-5}	t_{-4}	t_{-3}
t_{-2}	t_{-1}	s	t_{+1}	t_{+2}
t_{+3}	t_{+4}	t_{+5}	t_{+6}	t_{+7}
t_{+8}	t_{+9}	t_{+10}	t_{+11}	t_{+12}

Fig. 7.2 Point s and its neighboring points t_i in the neighbor's area N_s.

7.2 Noise Reduction with a Complex-Valued Cellular Neural Network

Then, how can the human brain easily estimate the shape of Mount Fuji? Human beings first estimate the shape roughly and globally. Afterwards, if we find an inconsistent point in a precise examination of the phase map, we will presume a correct pixel value in a pattern processing by observing the surrounding pixels, and will remove the SP.

In this chapter, we present a neural network that performs a task such as the "phase-familiar brain" does. It is a superbrain named complex Markov-random-field (CMRF) estimating neural network (See Section 4.6) which is constructed as a complex-valued cellular neural network. A cellular neural network has neurons at lattice points, and a neuron has connections only locally. A two-dimensional cellular network is suitable for image processing and compatible with integration on a chip.

In phase unwrapping, we may use only phase data in general. However, the present complex-valued network deals with not only the phase but also the amplitude, as complex amplitude consistently, of the image data because, in many cases, they are related closely to each other. As we mentioned above, they are correlated strongly in particular at around an SP. We utilize the amplitude information effectively.

The network estimates a correct pixel value at a detected SP by using the values around the SP, and modifies the pixel value based on the estimate. This process reduces the number of SPs considerably, lightens the calculation cost required in making a DEM, and improves the DEM quality [194],[203],[198].

In the same manner as we did in Chapter 5, we label the pixels as shown in Fig.7.2. We adopt the CMRF model. Remember that, when we consider a probability $P(z_s)$ that the pixel s has a value of z_s

$$P(z_s| \text{ values of pixels in the image except for } s \ ) = P(z_s|z_{t_i} \in N_s) \quad (7.1)$$

where $t_i \in N_s$ is neighbors, the probability can be assumed constant in an area with a certain extension and, consequently, it represents a nature of the image statistically.

Accordingly, the value at the pixel s is estimated statistically by the neighbors. In the conventional real-valued MRF model, the probability P_s that the pixel s takes the value of x_s is estimated by the neighbor values x_t as

$$P(x_s) = \frac{1}{Z} e^{-E(x_s)} \tag{7.2}$$

$$E(x_s) = \frac{1}{2\sigma^2} \left(x_s - \sum_{t \in N_s} \Lambda_{st}^{\mathrm{T}} x_t \right)^2 \tag{7.3}$$

where Z is the partition function for normalization, Λ_{st} ($= w_{st}$ in Section 4.6) is correlations in a generalized-inverse-matrix expression, σ^2 is variance reflecting the degree of fluctuation, and $E(x_s)$ is energy. The parameters Λ_{st} and σ^2 are called the MRF parameters.

We extend the formula into a complex one to extract statistic features and to estimate pixel values of complex-valued images. We derive the complex-valued version for a complex pixel value z_s, by considering an analogy with the real-valued one given above and substituting conjugate transpose for simple transpose, as [194]

$$P(z_s) = \frac{1}{Z} e^{-E(z_s)} \tag{7.4}$$

$$E(z_s) = \frac{1}{2\sigma^2} \left| z_s - \sum_{t \in N_s} \Lambda_{st}^{*} z_t \right|^2 . \tag{7.5}$$

However, in practice, we have to estimate the CMRF parameters Λ_{st}^{*} based on the data in a local area. By considering averages within an $L \times L$ local observation area, we estimate the CMRF parameters as

$$\hat{\boldsymbol{\Lambda}}^{*} \equiv \left[\sum_{s \in L \times L} z_s \boldsymbol{q}_s^{*} \right] \left[\sum_{s \in L \times L} \boldsymbol{q}_s^{*} \boldsymbol{q}_s \right]^{-1} \tag{7.6}$$

$$\hat{\sigma}^2 \equiv \frac{1}{L^2} \sum_{s \in L \times L} \left| z_s - \hat{\boldsymbol{\Lambda}}^{*} \boldsymbol{q}_s \right|^2 \tag{7.7}$$

$$\boldsymbol{q}_s \equiv \begin{bmatrix} z_{t_{-12}} \\ z_{t_{-11}} \\ \vdots \\ z_{t_{+11}} \\ z_{t_{+12}} \end{bmatrix} \tag{7.8}$$

Note that, in the above expression, we omit the suffix st of $\hat{\boldsymbol{\Lambda}}^{*}$ since we estimate the parameters finally for arbitrary s by scanning the local area by shifting s and N_s.

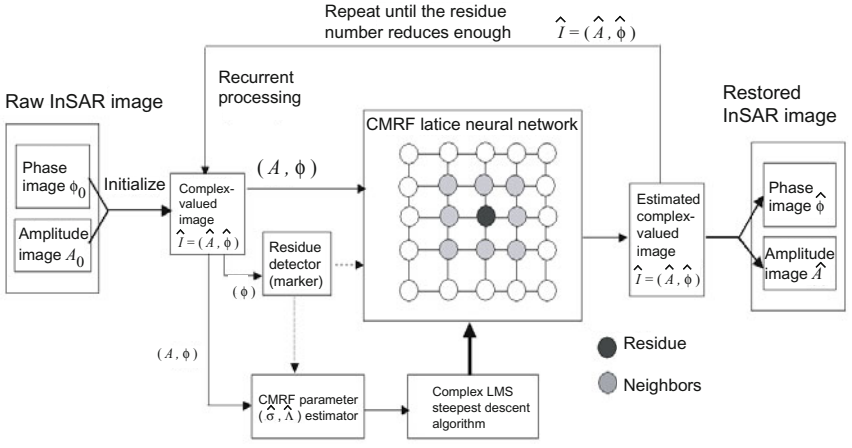

Fig. 7.3 Construction of the complex-valued cellular neural network to remove singular points. (Reprinted from Fig.4 in [194]: Andriyan Bayu Suksmono and Akira Hirose: Adaptive noise reduction of InSAR image based on complex-valued MRF model and its application to phase unwrapping problem, *IEEE Trans. on Geoscience and Remote Sensing,* 40(3):699–709 (followed by publisher's errata on Fig.12), 2002 ((C) 2002 *IEEE*) with permission from the IEEE.)

In (7.6), we obtain the estimate of z_s by using $\hat{\mathbf{\Lambda}}^*$ obtained as a generalized-inverse matrix described in Chapter 4. However, fundamentally we can estimate the parameters $\hat{\mathbf{\Lambda}}^*$ by employing the simple complex-valued Hebbian rule. That is to say, we can do it with the neural Hebbian (correlation) learning as $\hat{\mathbf{\Lambda}}^* = \sum z_s \boldsymbol{q}_s^*$, which has the same nature as the CMRF parameters expressed by (7.6). In other words, we can explain the process to estimate the CMRF parameters as a self-organization in the cellular neural network where a neuron is assigned to every pixel, and neural connections between neurons learn the correlation between the pixel values as $< z_s(z_t)^* >$. When the neighbor window N_s scans the local area in which the statistic property is unchanged, the network self-organizes to realize the estimation of the CMRF parameters similar to those expressed in (7.6).

7.3 System Construction

Figure 7.3 shows the system construction. A complex-valued reflection image $\boldsymbol{I}$ is input from the left-hand side. In the reflection observation, a homodyne circuit yields in-phase (real-part) and quadrature-phase (imaginary-part) components. Thereby, we regard the phase of the local oscillator output as the phase reference. If we use a vector network analyzer, we may obtain

directly the phase and amplitude of the reflection. In any case, by scanning the beam direction, we obtain a complex-valued reflection image $\boldsymbol{I}$.

We scan the image $\boldsymbol{I}$ and detect SPs. At the same time, we estimate the CMRF parameters $(\hat{\rho}^2, \hat{\Lambda})$ by using the data in the area containing no SPs. Then, as shown in the large rectangle at the center in Fig.7.3, we update the pixel value at the SPs. That is, the neuron at an SP connected locally to other neurons estimate the proper pixel value based on the CMRF parameters $(\hat{\rho}^2, \hat{\Lambda})$ and the surrounding pixel values. We modify the pixel value in such a manner that the energy expressed in (7.5) is reduced. We can employ a deterministic method [194], or a probabilistic hill-climbing one [203].

We update the pixel values at all the SPs to obtain a first estimate image $\hat{\boldsymbol{I}}$. We can expect that the number of the SPs in the estimate is less than that in the initial image. By repeating the above process, we generate a final estimate image $\hat{\boldsymbol{I}}$.

7.4 Dynamics of Singular-Point Reduction

Figure 7.4 shows the detail of the SP reduction. In Fig.7.4(a), we find observed amplitude and phase images with a corresponding SP map from the left-hand side to the right. The values of the amplitude and phase images are expressed in grayscale. There are two types of SPs, i.e., counterclockwise increasing SPs (positive SPs) and clockwise increasing SPs (negative SPs). They are

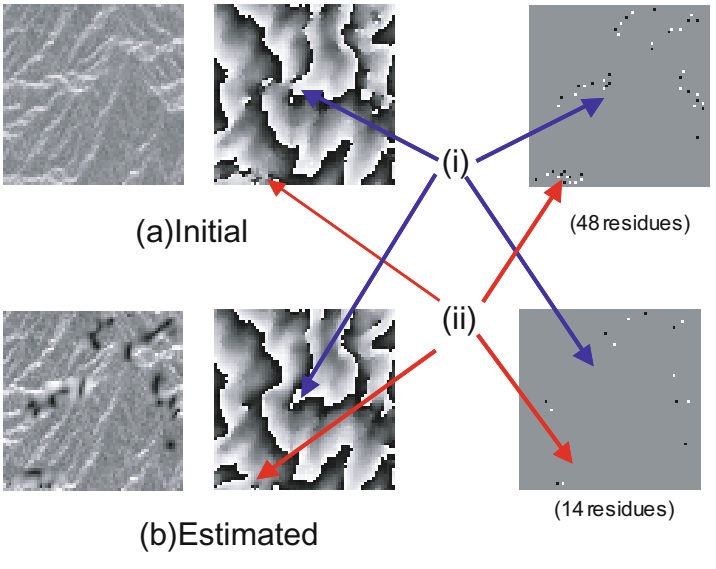

Fig. 7.4 Close-up of amplitude and phase images with a corresponding SP map from the left-hand side to the right. (Reprinted from Fig.6 in [194] in figure caption of Fig.7.3 ((C) 2002 *IEEE* with permission, IEEE.)

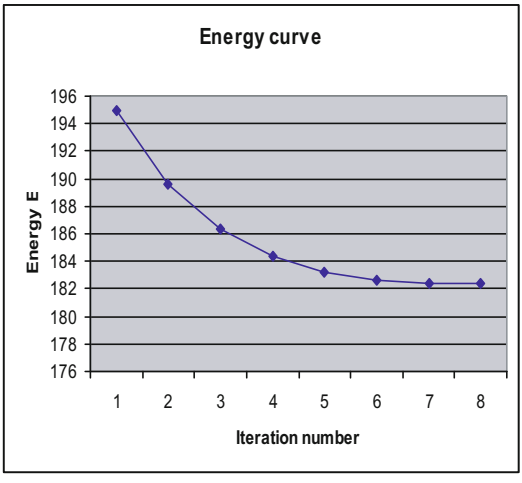

Fig. 7.5 Energy versus iteration number. (Reprinted from Fig.7 in [194] in figure caption of Fig.7.3 ((C) 2002 *IEEE* with permission, IEEE.)

expressed by white and black dots, respectively, in the SP map, where we have 48 SPs in this case in total. On the other hand, Fig.7.4(b) shows the processing result. We find that the number of the SPs is reduced to 14, and that the phase image has almost the same contours as those in the observed phase image in (a). In a close observation at the areas indicated by (i) and (ii), it is clear that the proposed neural network removes the SPs and, at the same time, the global elevation information is preserved. In the amplitude image in (b), the amplitude values around the SPs are modified to approximately zero in a wider area so that, as we considered in Section 7.1, the physical consistency is maintained explicitly around the SPs where the phase values cannot be determined uniquely.

Figure 7.5 presents the energy value defined in (7.5) versus the number of iteration of the neural processing. It decreases monotonically, which suggests a successful removal of the SPs.

7.5 DEM Quality and Calculation Cost

Figure 7.6 shows the results for an observation at the Mount Fuji area [194]. Figure 7.6(a) is the case where we apply the branch-cut method directly to the observed phase image. There we find the phase image, corresponding minimum-spanning-tree branch-cut, and obtained DEM. The DEM is expressed in color, where purple means undefined height because of closed branch-cut.

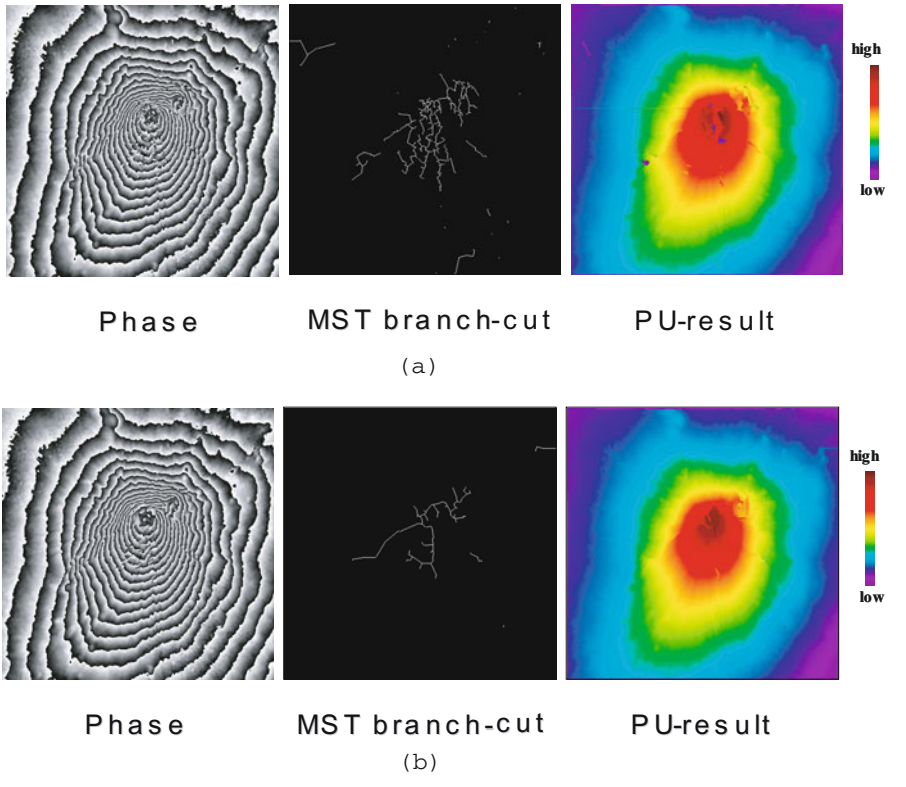

Fig. 7.6 Results for Mount Fuji observation: (a)Observed phase image, minimum-spanning-tree branch-cut, and resulting DEM obtained directly from the observed phase image without SP reduction, and (b)phase image after SP reduction, corresponding minimum-spanning-tree branch-cut, and resulting DEM obtained for the SP-reduced complex-amplitude image. (Reprinted from Figs.10, 12, 13, and 14 in [194] in figure caption of Fig.7.3 ((C) 2002 *IEEE* with permission, IEEE.)

On the other hand, Fig.7.6(b) shows the results when we conducted the SP reduction with the complex-valued cellular neural network. Though we cannot find difference between the phase images in (a) and (b) at a glance, the SP number in (a) is 611, while that in (b) has been reduced to just 100. That is to say, the neural processing realizes a great SP reduction without global landscape modification. Consequently, the total length of the branch-cut in (b) has become so short that the resulting DEM contains only small unnatural areas. The calculation time required for the branch-cut phase-unwrapping process has also been reduced to approximately 1/8.5.

7.6 Summary

In this chapter, we presented a complex-valued cellular neural network to estimate pixel values based on the complex-valued Markov random field (CMRF) model. At around singular points (SPs), the network estimates correct complex-amplitude reflection values, and reduces the number of the SPs. As a result, the calculation cost in the branch-cut phase unwrapping (PU) is drastically reduced. The quality of the obtained DEM is also greatly improved. The present estimation technique based on statistics is useful when the statistical property is considered almost uniform in a local area. In the Mount Fuji case, the statistics changes in the image in total. However, by preparing a local area smaller than the spatial changes of the statistic characteristics, we have been successful in applying the present method very effectively. Note that it is quite important that we deal with the phase together with the amplitude, i.e., the complex-amplitude, even if we are finally interested only in phase information.

The method presented here has advanced into an improvement in the works of Yamaki & Hirose [146] in the first years of 2000s, where they deal with the four pixels constructing a singular point simultaneously, and also lead to new unwrapping techniques such as the "progressive least-square unwrapping method" (Suksmono & Hirose) [144] and the so-called "singularity spreading phase unwrapping (SSPU) method" (Yamaki & Hirose) [145]. Their practical applicability has been evaluated by, e.g., Japan Aerospace Exploration Agency (JAXA) for the near-future use in the world.